A&A 485, 417–424 (2008)
DOI: 10.1051/0004-6361:20077569

Astronomy & Astrophysics

Seyfert galaxies in the local Universe ($z \leq 0.1$): the average X-ray spectrum as seen by *BeppoSAX*

M. Dadina[1,2]

[1] INAF/IASF-Bo, via Gobetti 101, 40129 Bologna, Italy
[2] Dipartimento di Astronomia dell'Università degli Studi di Bologna, via Ranzani 1, 40127 Bologna, Italy
e-mail: mauro.dadina@iasfbo.inaf.it

Received 29 March 2007 / Accepted 6 February 2008

ABSTRACT

The *BeppoSAX* archive is currently the largest reservoir of high sensitivity simultaneous soft and hard-X ray data of Seyfert galaxies. From this database all the Seyfert galaxies (105 objects of which 43 are type I and 62 are type II) with redshift lower than 0.1 have been selected and analyzed in a homogeneous way. Taking advantage of the broad-band coverage of the *BeppoSAX* MECS and PDS instruments (~2–100 keV), the X-ray data so collected allow us to infer the average spectral properties of nearby Seyfert galaxies included in the original sample and, most notably the photon index ($\Gamma \sim 1.8$), the high-energy cut-off ($E_c \sim 290$ keV), and the relative amount of reflection ($R \sim 1.0$). The data collected have been used to test some basic assumptions of the unified scheme for active galactic nuclei. The distributions of the isotropic indicators used here (photon index, relative amount of reflection, high-energy cut-off and narrow FeKα energy centroid) are similar in type I and type II objects while the absorbing column and the iron line equivalent width significantly differ between the two classes of active galactic nuclei with type II objects displaying larger columns ($N_H \sim 3.7 \times 10^{22}$ and 6.1×10^{23} cm^{-2} for type I and II objects respectively) and equivalent width ($EW \sim 220$ and 690 eV for type I and II sources respectively). Confirming previous results, the narrow FeKα line is consistent, in Seyfert 2, with being produced in the same matter responsible for the observed obscuration. These results support the basic picture of the unified model. Moreover, the presence of a X-ray Baldwin effect in Seyfert 1 has been measured using the 20–100 keV luminosity ($EW \propto L(20\text{–}100)^{-0.22\pm0.05}$). Finally, the possible presence of a correlation between the photon index and the amount of reflection is confirmed thus indicating thermal Comptonization as the most likely origin of the high energy emission for the active galactic nuclei included in the original sample.

Key words. X-rays: galaxies – galaxies: Seyfert: – galaxies: active

1. Introduction

The high energy emission from active galactic nuclei (AGN) is thought to come from the innermost regions of accreting systems that are centered around super-massive black-holes (SMBH). For this reason, X-rays are expected to be tracers of the physical conditions experienced by matter before disappearing into SMBH. Moreover, thanks to their high penetrating power, energetic photons, escaping from the nuclear zones, test the matter located between their source and the observer. Thus, they offer powerful diagnostics to understand the geometry and the physical conditions of the matter surrounding the SMBH.

The broad-band of *BeppoSAX* offered for the first time the opportunity to measure with a remarkable sensitivity the spectral shape of AGN in the 0.1–200 keV range. This potential had been previously exploited to study in detail a number of sample selected in different manners (see for example Maiolino et al. 1998; Malizia et al. 2003; Perola et al. 2002). These studies were fundamental in making important steps forward in the comprehension of the emitting mechanism at work in the production of X-rays (Perola et al. 2002) and to partially reveal the geometry of the cold matter surrounding the central SMBH (Maiolino et al. 1998; Bassani et al. 1999; Risaliti et al. 1999).

The *BeppoSAX* database full potential, however, was never exploited before. In a previous paper, the entire catalog of the Seyfert galaxies at $z \leq 0.1$ contained in the *BeppoSAX* archive has been presented (Dadina 2007). This sample was selected starting from the catalog of Seyfert galaxies contained in the Véron-Cetty & Véron (2006) sample of AGN and contains 13 radio-loud objects and 7 narrow-line Seyfert 1.

The spectral analysis was performed in the 2–100 keV band whenever possible and the data were fit with a set of template models to obtain a homogeneous dataset. Here the X-ray data so collected are statistically inspected to infer the average characteristics of the nearby Seyfert galaxies contained in this sample in the 2–100 keV band. Finally, the present dataset is used to perform simple tests on the unified scheme (UM) for the AGN (Antonucci 1993) and on the emission mechanism acting in the core of the Seyfert galaxies. More detailed analysis on this latter topic will be presented in another paper (Petrucci et al., submitted) where detailed thermal Comptonization models (Poutanen & Svensson 1996; Haardt & Maraschi 1993) will be used to fit the BeppoSAX data to study the dependence of the spectral properties in the "two phase" scenario (Haardt 1991; Haardt & Maraschi 1993) assuming different geometries of the corona.

2. Mean X-ray properties

The scope of this section is to determine and study the mean X-ray spectral properties of the sample and to use these values to test the UM model for AGN (Antonucci 1993). The key parameters are the ones that describe the continuum and the absorption properties. In the framework of the UM models for AGN, the

continuum shape is expected to be independent to the orientation angle under which the source is observed. Thus, no difference should be measured in the parameters describing the continuum between type I and II objects. On the contrary, the absorbing column intervening in Seyfert 2 should be the principal discriminator between the two classes of objects. Thus measuring the mean X-ray properties is a test of the basic assumptions of the UM.

2.1. Methods

The origins of the X-ray photons from AGN are thought to be due to Comptonization of optical-UV radiation, coming from the accretion disk and Comptonized by the e^- in the hot corona that sandwiches the disk (Haardt & Maraschi 1991; Haardt 1993; Poutanen & Svensson 1996; Czerny et al. 2003). The mechanism is assumed to be, at least at the zero-th order, very similar in each Seyfert galaxy. Under this hypothesis, the differences between the X-ray spectra of different objects are supposed to be mainly due to two kind of factors: i) the time-dependent state of the emitting source; ii) the intervening matter that imprints on the emerging spectrum the features typical of its physical state. In such a scenario, the observations of many sources can be regarded as the long-term monitoring of a single source. On the other hand, it is also true that the contrary has some comparison in the literature: e.g. time sparse observations of a single source in different states can resemble observations of objects with completely different spectral properties. This is the case, for example, of the narrow line Seyfert 1 NGC 4051 that displayed variations in flux/luminosity by a factor of ∼100 (Guainazzi et al. 1998) associated with strong variations of the spectral shape ($\Gamma \sim 0.5$–2.4; Guainazzi et al. 1998; Turner et al. 1999; Ponti et al. 2006; but see also Crenshaw & Kraemer 2007, for a different interpretation of this spectral behavior in terms of variable ionized absorption). To calculate the mean X-ray properties of the sources included in this work I treated the multiple observations of single sources separately: i.e. I assumed different observations of the same source as if they were observations of different sources.

This method, in principle, is expected to work properly for all those quantities which are supposed to vary in accordance with the state of activity of the central nucleus. For example, the photon index Γ is known to vary with the AGN flux state (Lee et al. 2000; Shih et al. 2002; Ponti et al. 2006) and the high-energy cut-off (E_c) is linked with the temperature of the corona and thus expected to be variable (Haardt et al. 1997). On the contrary this method is not expected to work properly when constant components are considered. This could be the case, for instance, of the cold absorption assumed to be due to the putative dusty torus (Antonucci 1993). Thus, for this component, the average value recorded for each source should be used. Nonetheless, these components also were observed to vary in a number of objects (see for example the case of NGC 4151, De Rosa et al. 2006; or Risaliti et al. 2002). Moreover, the constancy of the properties of the cold absorption is predicted under the hypothesis of a continuous distribution of the matter that forms the torus. On the contrary, if the torus is formed of blobs/clouds (Elitzur & Shlosman 2006), variability in the measurements of the absorbing column is expected. For both these observational and theoretical reasons the N_H measured in each single observation were treated separately.

In between these two cases are the properties of the emission FeKα line. *BeppoSAX* had a too low sensitivity to detect the relativistically broadened component of this feature in a large number of sources. Thus only the narrow line has been detected in the vast majority of the objects included in the original catalog. This component is supposed to originate far from the SMBH, at least at ∼1000 Schwarzschild radii (Mattson & Weaver 2004), i.e. very likely at the inner edge of the torus (Nandra 2006). At these distances from the SMBH, the relativistic effects are negligible. Thus, in principle, the parameters that describe the line should be regarded as stable. Nonetheless the properties of the narrow FeKα line were also observed to vary with its line energy centroid changes between ∼6.4 keV (neutral iron) and ∼6.9 keV (H-like iron) showing different ionization states. Moreover, the equivalent width (EW) of this component is not only a function of the intensity of the line itself, but it is also directly linked to the underlying variable continuum emitted in the regions close to the SMBH. This makes EW a variable quantity. The parameters of the emission FeKα line were thus treated as variable ones in order to test its origin, and not averaged when objects were observed more than once.

Finally, in a number of cases it was necessary to deal with censored data (see Table 1). To manage these data properly, the ASURV software (Feigelson & Nelson 1985; Isobe et al. 1986) was used. In particular, to establish if the distributions of parameters of type I and type II objects were drawn from different parent populations, the Peto & Prentice generalized Wilcoxon test (Feigelson & Nelson 1985) has been used while to calculate the mean values considering also the censored data the Kaplan-Meyer estimator was used. To establish the presence of correlations between different quantities, both the Spearman's ρ and the generalized Kendall's τ methods were applied. The linear regressions were calculated using the Bukley-James and Schmitt's methods. In the following, two quantities are considered as drawn from different parent populations when the probability of false rejection of the null hypothesis (same parent population) is $P_{null} \leq 1\%$. Similarly, one accepts that there is a correlation between two given quantities when the probability of an absence of correlation remains lower than 1%.

Table 1. General characteristics of the data analyzed in this work. The number of detections and censored data are reported for the interesting parameters for the whole sample of objects (Cols. 2 and 3), for the Seyfert 1 galaxies (Cols. 4 and 5), and for the Seyfert 2 objects (Cols. 6 and 7). The 90% confidence interval limits were used for censored data and the detected values were defined if determined with a 99% confidence level (Dadina 2007)

Parameter	Tot. Sample		Seyfert 1		Seyfert 2	
	Det.	Cens.	Det.	Cens.	Det.	Cens.
N_H	83	80	31	53	52	27
EW	129	7	66	4	63	3
R	68	18	46	9	22	9
E_c	33	51	27	26	6	25

2.2. The X-ray continuum and the cold absorption

The X-ray continua of the sources have been modeled using a cut-off power-law that describes the primary emission from the hot corona plus a reflection component (*PEXRAV* model in Xspec, Magdziarz & Zdziarski 1995) to account for the contribution expected to be due to the disk. However, an additional reflection component could rise from the torus (Ghisellini et al. 1994) and the disentangling between the two reflection components is impossible with the quality of the available data. Wherever its origin, the reflection has been assumed to be due to cold matter.

Table 2. Mean spectral properties. Col. I: Spectral parameter; Col. II: Seyfert 1 mean value; Col. III: Seyfert 2 mean value; Col. IV: Probability that Seyfert 1 and Seyfert 2 are drawn from the same parent populations.

Parameter	Tot.	Seyfert 1	Seyfert 2	$P_{\rm null}$
Γ	1.84 ± 0.03	1.89 ± 0.03	1.80 ± 0.05	90%
R	1.01 ± 0.09	1.23 ± 0.11	0.87 ± 0.14	5%
$E_{\rm c}$ †	287 ± 24	230 ± 22	376 ± 42	5%
$N_{\rm H}$ ‡	31.7 ± 9.1	3.66 ± 2.34	61.3 ± 18.0	≤0.1%

† In units of eV; ‡ in units of 10^{22} cm^{-2}.

The interesting parameters are the photon index (Γ), the relative amount of reflection (R), and the high-energy cut-off ($E_{\rm c}$).

In Table 2 the results for the whole set of observations and for the two classes of Seyferts are reported as well as the probability that Seyfert 1 and 2 are drawn from the same parent populations. The histograms of the distributions of the interesting parameters for the entire sample of objects (first column) and for type I (second column) and type II (third column) are reported in Fig. 1.

As previously said, the UM for AGN (Antonucci 1993) predicts that Γ, R, and $E_{\rm c}$ are observables independent of the inclination angle, thus the two classes of Seyfert galaxies should display very similar characteristics. This is confirmed by the analysis of the present sample. In particular, there are no hints that the distributions of photon index Γ for the two types of Seyfert are drawn from different parent populations ($P_{\rm null} \sim 90\%$). Moreover, the photon-index peaks, for both classes, between 1.8–1.9 in agreement with the two-phase models for the production of the X-ray in Seyfert galaxies that predict $\Gamma \sim 1.5$–2.5 (Haardt & Maraschi 1991; Haardt 1993; Haardt et al. 1997). Few objects have extremely flat spectra with $\Gamma \leq 1$. Type II objects that show such hard X-ray spectra are supposed to be Compton-thick sources for which, in the 2–10 keV band, only the reflected/flat spectrum is observable. This is the case for NGC 2273 which displays the harder X-ray spectrum. This source was first classified as a Compton-thick object by Maiolino et al. (1998). The Seyfert 1s with flattest spectra are NGC 4151 that is known to have a hard spectrum with complex and variable absorption (De Rosa et al. 2007) and Mrk 231 (classified as a type I AGN by Farrah et al. 2003). The latter source shows a very hard X-ray spectrum with $\Gamma \sim 0.7$. This source is also classified as a BAL QSO (Smith et al. 1995). A recent spectral analysis in the X-ray band of this source was presented in Braito et al. (2004). By combining *XMM-Newton* and *BeppoSAX* data, these authors speculated that the spectrum of the source below ∼10 keV is reflection dominated, thus presenting a case that is difficult to reconciled with the UM of AGN. Moreover, Mrk 231 is an ultra-luminous infra-red galaxy. These sources display strong starburst activity that can dominate the total X-ray luminosity of the galaxy (see Franceschini et al. 2003; Ptak et al. 2003, for details on this topic) although in Mrk 231 at least 60% of the observed 0.5–10 keV flux seems to be due to the AGN component (Braito et al. 2004).

Less conclusive results are obtained for R and $E_{\rm c}$. In both cases, the probability of false rejection of the null hypothesis (the two distributions are drawn from same parent populations, in accordance with the UM predictions), is $P_{\rm null} \sim 5\%$. However, both type I and II objects lie in the same range of R and $E_{\rm c}$. In particular, the distribution of R for type I objects is dominated by a peak of detections between $R \sim 1$–1.2 due to the contribution of a few sources observed several times (e.g. NGC 5548, IC 4329a). This has probably introduced a systematic effect not smeared-out by the relatively small number of useful observations (i.e, the ones for which R and $E_{\rm c}$ have been estimated). On the other hand, the result on $E_{\rm c}$ is most probably polluted by the large number of lower limits for Seyfert 2. If the same test is performed only on the detections it is obtained that $P_{\rm null} \sim 35\%$, making impossible to assess that the two samples are drawn from two different populations.

The result is unambiguously in accordance with UM predictions for the absorbing column. In this case the statistical tests confirm that Seyfert 1 and Seyfert 2 display very different absorption characteristics with the type II objects being more heavily absorbed than Seyfert 1. Again, it is noticeable that a few type I objects show high column densities (up to $\sim 10^{24}$ cm^{-2}) and some Seyfert 2 have low columns (down to 10^{21} cm^{-2}). These are not new results: the high column of NGC 4151 ($\sim 5 \times 10^{22}$, De Rosa et al. 2007) is well known. The highest column measured in a Seyfert 1 is detected during the June 9, 1998 observation of NGC 4051. During this observation the source appeared "switched-off" and only a pure reflection component was measured (Guainazzi et al. 1998). The spectral fit in Dadina (2007) degenerated between two solutions, one in which the source was purely reflection-dominated ($R \geq 7$) and a second one in which a direct component was visible but highly absorbed. The latter scenario was slightly preferred from a pure statistical point of view when the 2–200 keV band is condidered, and, for homogeneity, entered in the catalog (Dadina 2007). Nonetheless, when the entire *BeppoSAX* band (0.1–200 keV) is considered, the reflection scheme is preferred (Guainazzi et al. 1998).

Finally, a number of objects show upper-limits to the absorbing column of the order of $\sim 10^{22}$ cm^{-2}. This is a selection effect induced by the energy band considered using only MECS and PDS data (∼2–100 keV, Dadina 2007). The low-energy cut-off due to such a column (10^{22} cm^{-2}) peaks at $E \sim 2$ keV and only for those objects with good statistics it is possible to infer upper limits on the $N_{\rm H}$ below 10^{22} cm^{-2}. This is most probably responsible for the high value obtain for the average $N_{\rm H}$ in type I objects.

3. Probing the origin of the FeKα emission line

The FeKα line is produced by reprocessing the primary X-ray emission in matter surrounding the source of hard photons. In the framework of the UM, the origin of this component can be placed in a number of regions such as the accretion disk, the dusty torus, and the broad-line regions (even if this last hypothesis is disfavored by the recent results obtained with the *XMM-Newton* and *Chandra* observatories and presented in Nandra 2006). If the line originates in the disk close to the SMBH, relativistic effects that broaden the resulting line are expected. For the vast majority of the sources included in the original sample, only narrow components of such features were detected and only in a few cases broad emission lines (e.g. IC 4329a) or relativistically blurred features were detected (for example in MCG-6-30-15). Thus, the results presented here are essentially based on the measured properties of the narrow features.

As shown in Fig. 2 (first row), the line energy centroid is peaked at ∼6.4–6.5 keV (see also Table 3) in both type I and II objects. The centroid is slightly above 6.4 keV but, considering the energy resolution of the instrument at these energies (∼200 eV FWHM, Boella et al. 1997), the results obtained here are in agreement with the line being mainly produced in cold or nearly cold matter (ionization state below FeXVII), i.e. in

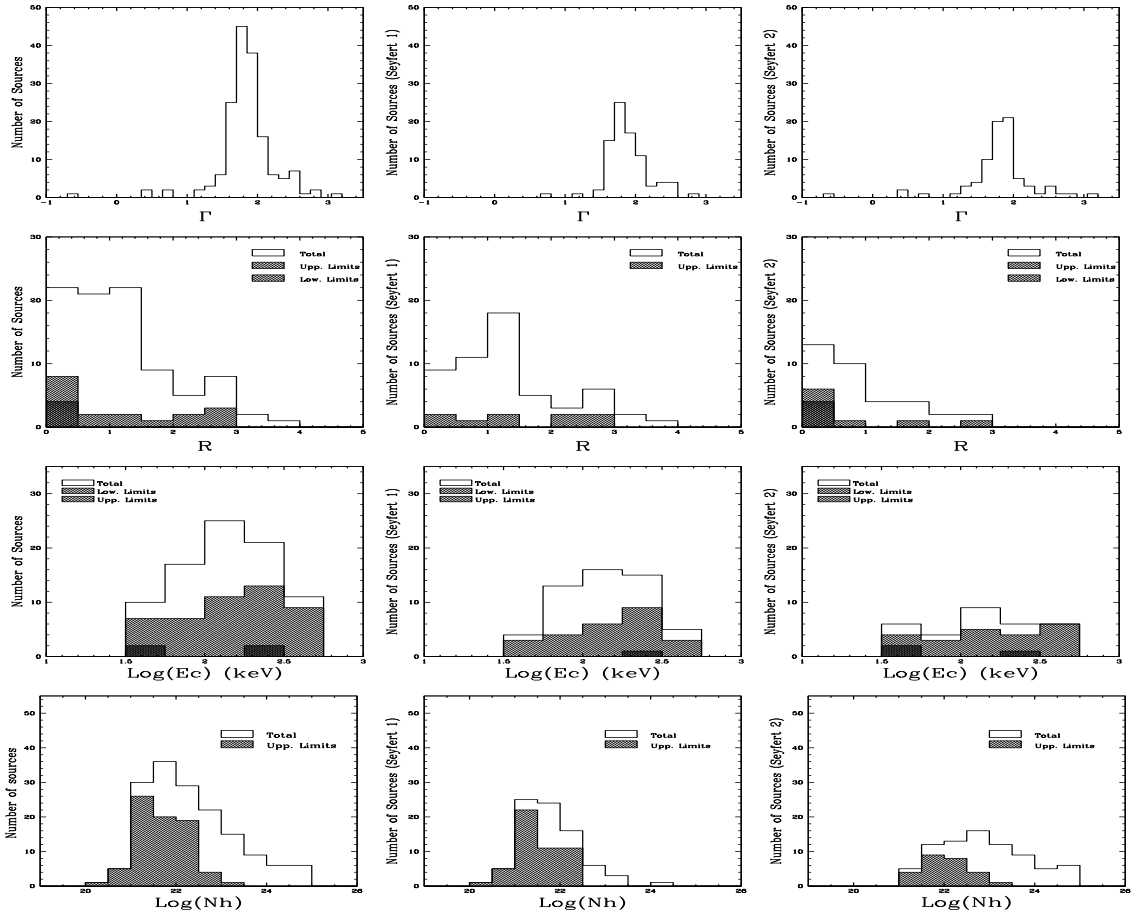

Fig. 1. Photon index Γ (*first row*), *R* (*second row*), E_c (*third row*), and N_H (*fourth row*) in units of cm^{-2} distributions for the whole dataset (*left column*), for type I objects (*center column*), and for type II objects (*right column*).

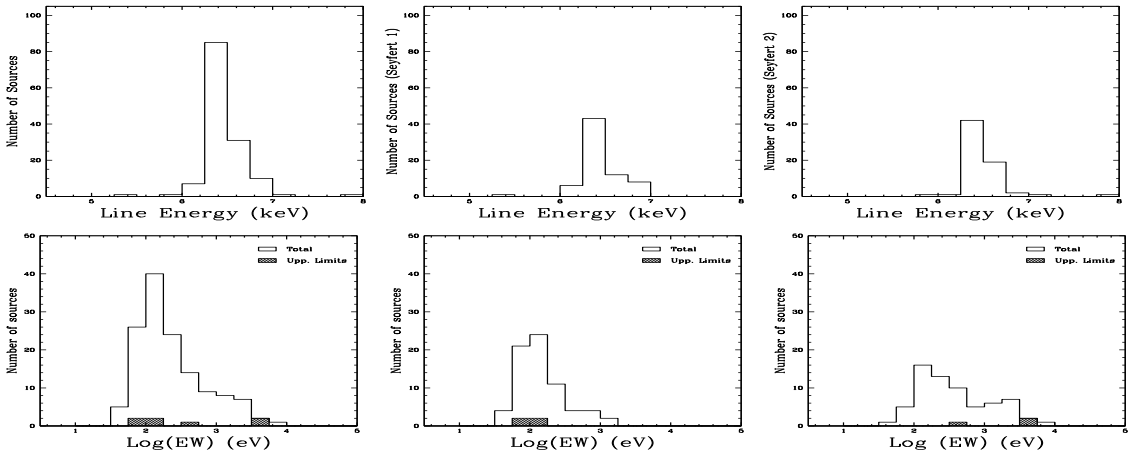

Fig. 2. Distribution of the Fekα emission line energy centroid (*first row*) and of its *EW* (*second row*). Distributions for the whole sample of observations (*left panel*), for the type I objects (*center panel*) and for type II objects (*right panel*).

both type I and II objects, by matter in the same physical state. However, a well known difference between the two classes of objects is the *EW* of the narrow FeKα line in type II objects, which shows stronger features than type I objects (see second row of Fig. 2 and Table 3, Bassani et al. 1999; Risaliti et al. 1999; Cappi et al. 2006; Panessa et al. 2006). As shown in the central panel of Fig. 2, the Seyfert 1s peak at $EW_{\mathrm{FeK}\alpha} \sim$ 100–200 eV while the type II have a broader distribution with a hard tail that reaches values well above 1 keV. Also few Seyfert 1 have large values of *EW* of the FeKα line (above 300–400 eV). The large *EW* tail of the Seyfert 1 distribution is composed mainly of objects in which the broad components of the FeKα line are detected such as in MCG-6-30-15, Mrk 841 and IC 4329a. The Seyfert 1 with largest *EW* is NGC 4051 during the June 9, 1998 observation when its spectrum was due to pure reflection (Guainazzi et al. 1998).

The larger FeKα *EW* in Seyfert 2 galaxies is in agreement with the UM (Antonucci 1993). If the origin of this component

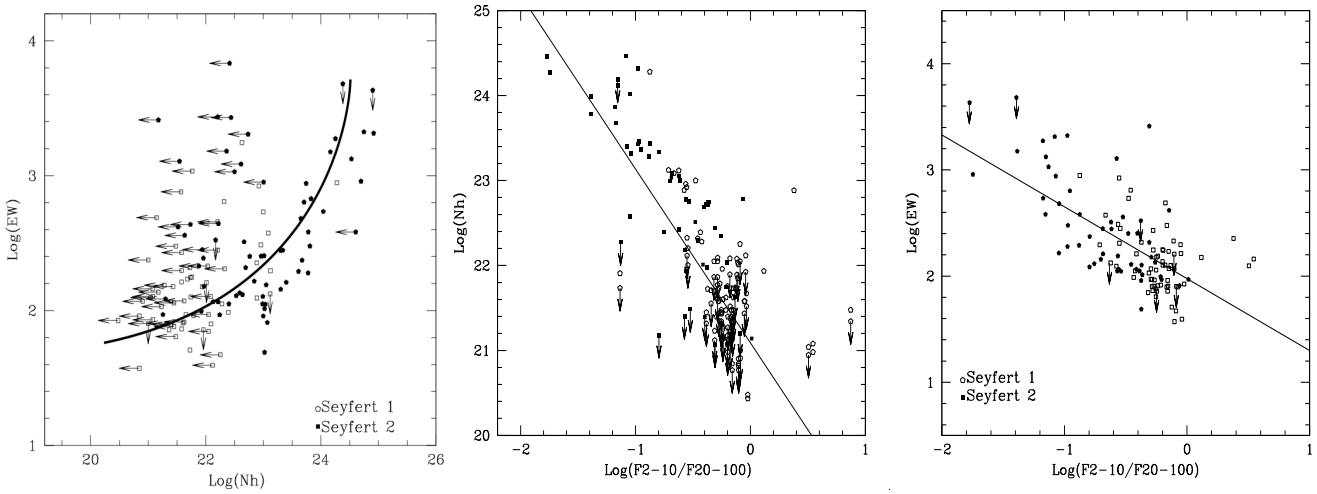

Fig. 3. *Left panel*: Log ($EW_{\mathrm{FeK}\alpha}$) vs. Log (N_{H}). As expected, the sources are divided in two families: the ones that follow the expectations if the FeKα line is produced in the absorption matter and the candidate Compton-thick ones that display low absorption and large *EW*. The solid line indicates the prediction by Makishima (1986). *Center panel*: Log ($F_{2-10\ \mathrm{KeV}}/F_{20-100\ \mathrm{KeV}}$) vs. Log ($N_{\mathrm{H}}$). The two quantities are correlated as expected since the 2–10 keV band is strongly affected by the absorption while the 20–100 band is almost free from absorption. The solid line is the best fit obtained with linear regression methods *Right panel*: Log ($EW_{\mathrm{FeK}\alpha}$) vs. Log ($F_{2-10\ \mathrm{KeV}}/F_{20-100\ \mathrm{KeV}}$). The two quantities are strongly correlated ($P_{\mathrm{null}} \leq 0.01$). The ratio between X-ray fluxes is a model independent indicator of the absorption affecting the low energy band. Thus, this correlation strongly indicates that the narrow component of FeKα line in emission is indeed produced by the same matter responsible for the absorption. The solid line is the linear regression obtained using Bukley-James method (Isobe et al. 1986).

Table 3. Mean properties of the FeKα emission line. Column I: spectral parameter; Column II mean value for the whole sample; Column III: mean value for Seyfert 1; Column IV: mean value for Seyfert 2. Column V: Probability that the parameters of type I and type II objects are drawn from the same parent population.

Parameter	Tot.	Seyfert 1†	Seyfert 2†	P_{null}
$E^{\dagger}_{\mathrm{FeK}\alpha}$	6.49 ± 0.02	6.46 ± 0.03	6.51 ± 0.03	32%
$EW^{\ddagger}_{\mathrm{FeK}\alpha}$	448 ± 67	222 ± 33	693 ± 195	≤1%

† In units of keV; ‡ in units of eV.

is indeed located in the dusty torus, than the line *EW* has to be correlated with the absorber column density. This is indeed what is observed also in this sample (see Fig. 3, left panel). Moreover, the Spearman ρ and Kendall's τ tests indicate that a correlation between the FeKα *EW* and the N_{H} is highly probable for type II objects ($P_{\mathrm{null}} \leq 0.1\%$), i.e. for that sources for which we can have direct evidence of the torus absorbing column. The robustness of the N_{H} estimates have been tested by correlating it with the model independent indicator offered by the ratio of the observed fluxes at 2–10 and 20–100 keV respectively (center panel of Fig. 3). The two quantities are strongly correlated (generalized Spearman ρ and Kendal τ tests give $P_{\mathrm{null}} \leq 0.1\%$) with only a few exceptions: the pure Compton-thick sources which are located in the diagram below the majority of the sources. This effect is expected since the absorbing column can affect the X-ray radiation below ∼10 keV while at harder energies the radiation pierces the matter for columns ≤3–5 × 10^{24} cm^{-2}. Otherwise, the Compton absorption dominates and also photons with energy above 10 keV are stopped since the Klein-Nishina regime is reached.

As stated above, when the *EW* of the FeKα emission line is tested against the measured N_{H} (left panel of Fig. 3) a result in good agreement with what is predicted by theoretical models is obtained (Makishima 1986; Leahy & Creighton 1993). The majority of the sources, in fact, behave as expected if the line is produced by the absorbing matter that depresses the direct continuum (Makishima 1986). All the known Compton-thick sources are located at low N_{H} and high *EW*, in accordance with previous results (Bassani et al. 1999; Risaliti et al. 1999). As an additional test, the *EW* of the FeKα line has been plotted versus the $F_{2-10\ \mathrm{KeV}}/F_{20-100\ \mathrm{KeV}}$ ratio. As expected (see right panel of Fig. 3), a good correlation ($P_{\mathrm{null}} \leq 0.1\%$ according to generalized Spearman ρ and Kendall τ tests) is obtained.

These results thus confirm that the properties of the FeKα line agree with the expectations of the UM for AGN. Nonetheless, this is not the only information we have about the iron line. In recent papers (Iwasawa & Taniguchi 1993; Page et al. 2004; Grandi et al. 2006; Bianchi et al. 2007) it has been claimed that a X-ray "Baldwin effect" (or Iwasawa-Taniguchi effect) is present in AGN when the FeKα intensity is probed against the 2–10 keV luminosity. Here this effect is tested considering for the first time both the 2–10 keV and the 20–100 keV luminosities.

A strong correlation ($P_{\mathrm{null}} \leq 0.1\%$ using Spearman ρ and generalized Kendal τ test) is found when the *EW* of the FeKα line is plotted both against the observed 2–10 keV (panel (a) of Fig. 4) and 20–100 keV (panel (c) of Fig. 4) keV luminosities. The nature of these correlations, however, is not straightforward, especially for the 2–10 keV luminosity. In this energy band the effect of the absorber is very important. As previously demonstrated, the *EW* of the iron line correlates with N_{H}, but stronger absorbing columns imply lower fluxes. Moreover, when the relation between the FeKα line *EW* and the 2–10 keV flux is investigated (panel (b) of Fig. 4), it is found that the two quantities are correlated ($P_{\mathrm{null}} \leq 1\%$). This is explainable only in terms of instrumental effects, since the sensitivity of the instruments to narrow features decreases with the source's flux. Thus, to be detected in faint objects, the FeKα line must be strong enough. Since the original sample is limited to the local Universe, this correlation in flux acts, at least partially, also in the *EW* vs. $L_{2-10\ \mathrm{KeV}}$ relation.

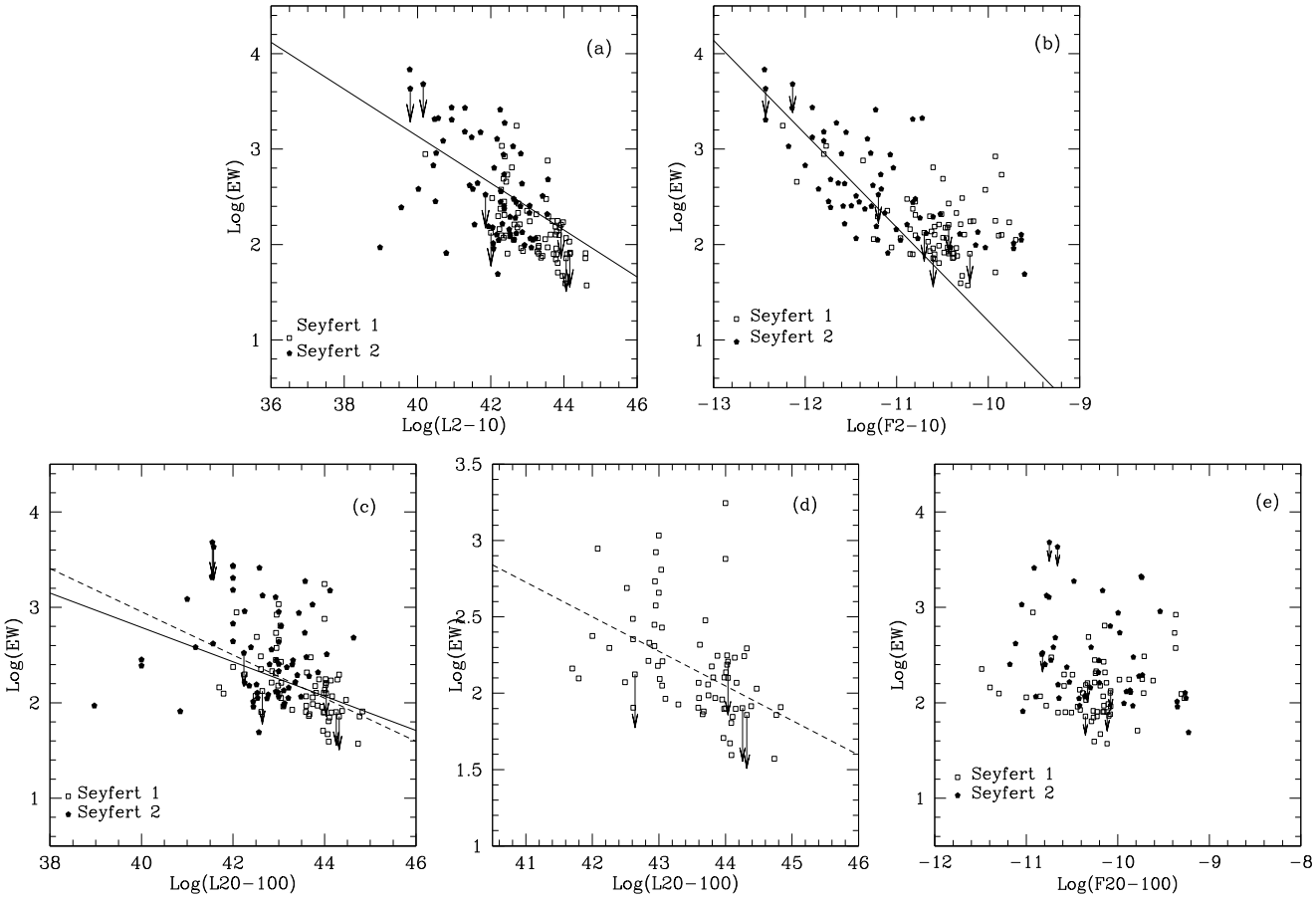

Fig. 4. Panel **a)**: Log $(EW_{\mathrm{FeK}_\alpha})$ vs. $L_{2-10,\,\mathrm{observed}}$. Panel **b)**: Log $(EW_{\mathrm{FeK}_\alpha})$ vs. $F_{2-10,\,\mathrm{observed}}$. Panel **c)**: Log $(EW_{\mathrm{FeK}_\alpha})$ vs. $L_{20-100,\,\mathrm{observed}}$. Panel **d)**: the same as panel **c)** but only for Seyfert 1 objects. Panel **e)**: Log $(EW_{\mathrm{FeK}_\alpha})$ vs. $F_{20-100,\,\mathrm{observed}}$. Solid lines in panel **a)**, **b)**, and **c)** are the linear regressions obtained for the whole sample of observations. The dashed line in panels **c)** and **e)** is the linear regression obtained considering only type I objects. As visible in panel **b)** the less scattered relation is obtained considering the 2–10 keV observed flux. The relation is linear, as expected if the correlation is due to selection effects, i.e.considering that in faint objects only large *EW* were detectable by the MECS instruments on-board *BeppoSAX*.

This N_{H} effect should be negligible when the 20–100 keV band is considered. In fact, in this case, one expects to find a correlation between the observed 20–100 keV luminosity and the *EW* of the FeKα line only in the most extreme cases, i.e. for the "pure Compton thick" objects. Apart from NGC 1068, these sources are too weak to be detected by the PDS, thus unable to drive the relation observed in plot (c) of Fig. 4. Moreover, panel (e) of Fig. 4 indicates that the *EW* of the iron line is not related to the 20–100 keV flux thus excluding that the "Baldwin effect" measured using the 20–100 keV band is due to instrumental selection effect as it happens for the $F_{2-10\ \mathrm{KeV}}$. On the other hand, in the 20–100 keV band the reflection-hump at ∼30–40 keV contributes to the observed flux. If the origin of the FeKα line is due to the same matter responsible of the reflection, one should expect that the *EW* of the iron line should increase as the reflection component augments the 20–100 keV flux (i.e. the iron line *EW* should correlate with the 20–100 keV flux). Thus, the net contribution of the reflection component should act in the opposite direction to that observed (i.e. larger iron line *EW* at smaller 20–100 keV flux). If the two classes of Seyfert galaxies are analyzed separately it is obtained that a strong correlation is found for Seyfert 1 ($P_{\mathrm{null}} \leq 0.1\%$ using both Spearman ρ and generalized Kendal τ tests, panel (d) of Fig. 4) while no correlation is evident for type II objects ($P_{\mathrm{null}} \sim 80\%$). This result is not unexpected since the *EW* of the obscured sources are boosted by the suppression of part of the underlying continuum. To conclude, the presence of a X-ray Baldwin effect for Seyfert 1 is unambiguously confirmed by the present data if the $L_{20-100\ \mathrm{KeV}}$ is considered and it has the following relation:

$$\mathrm{Log}\,(EW) = -(0.22 \pm 0.05) \times \mathrm{Log}\,(L_{20-100}) + 11.91 \pm 2.52. \quad (1)$$

The slope of the relation found in this work is in agreement with that previously obtained by Page et al. (2004) ($EW \propto (L_{2-10})^{-0.17\pm0.08}$) using a sample containing both radio-quiet and radio-loud objects. The present result is also consistent with that found by Zhou & Wang (2005) (who used a sample containing both radio-quiet and radio-loud objects finding $EW \propto (L_{2-10})^{-0.15\pm0.05}$) and Bianchi et al. (2007) (who used only radio-quiet objects obtaining $EW \propto (L_{2-10})^{0.17\pm0.03}$). On the contrary, Jiang et al. (2006), excluding the radio-loud AGN from a sample similar to the one used by Page et al. (2004), found that $EW \propto (L_{2-10})^{0.10\pm0.05}$. It is worth recalling here, that the the present sample is composed of both radio-loud and radio quiet sources (Dadina 2007). In particular, it contains 7 radio-loud Seyfert 1, and only for 5 of them are the 20–100 and iron line data available. Nonetheless, the presence of these sources in the sample does not affect the FeKα *EW* vs. L_{20-100} relation ($EW \propto (L_{2-10})^{0.21\pm0.05}$ excluding radio-loud type I objects).

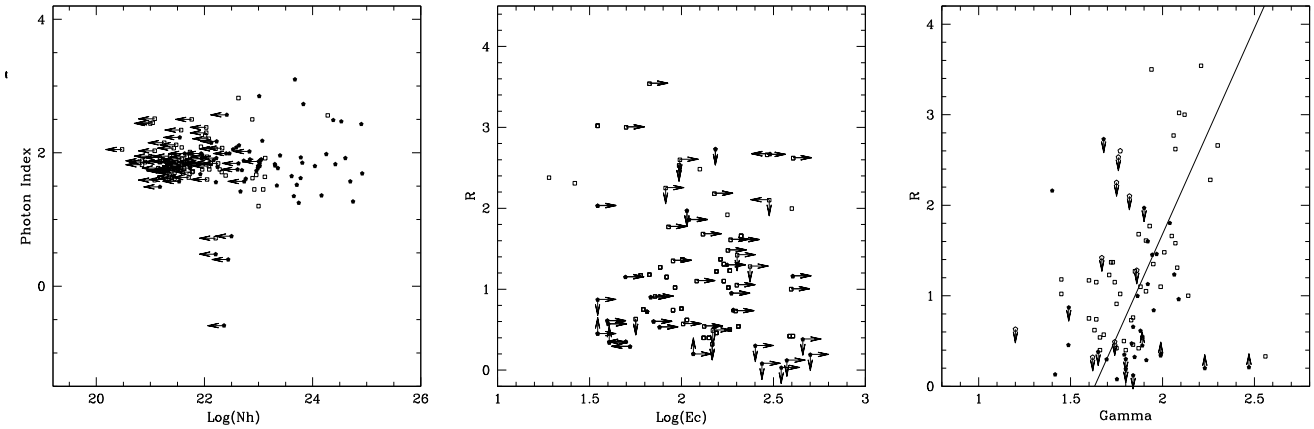

Fig. 5. *Left panel*: photon index Γ plotted versus the measured $N_{\rm H}$ (in units of cm^2). No significant trend relating these two quantities is found; *center panel*: R vs. $E_{\rm c}$ (in units keV), no correlation is found between these quantities; *right panel*: R vs. Γ. The two quantities are correlated with a high significance level ($P_{\rm null} \leq 1\%$). The line is the linear regression best fit.

The origin of the X-ray "Baldwin effect" is unclear. In the light bending scenario (Miniutti & Fabian 2004) the height of the source above the accretion disk determines the degree of beaming along the equatorial plane of the high energy emission. Because of relativistic effects, the closer the source is to the disk, the greater will be the fraction of X-rays beamed in the equatorial plane (i.e. towards the disk) and correspondingly lower will be the observed flux. Thus, the *EW* of the relativistically blurred FeKα line produced in the inner regions of the disk and the *EW* of the narrow iron line produced in the outer parts of the disk would appear enhanced in low-state sources.

On the contrary, Page et al. (2004) speculated that this effect could indicate that luminous sources are surrounded by dusty tori with lower covering factor thus pointings towards a torus origin of most of the narrow FeKα lines. The present work supports this view. The FeKα line *EW* of the iron line correlates with the observed $N_{\rm H}$ as predicted by theory (Makishima 1988; Lehay & Creighton 1993; Ghisellini et al. 1994). Moreover, the case ofthe extremely low state of NGC 4051 (Guainazzi et al. 1998) included in this dataset also seems to point in this direction. The very large *EW* of the narrow FeKα line recorded in this observation is typical of Compton-thick type II objects, but the line does not show evidence of relativistic broadening due to the contribution of the inner orbits of the accretion disk.

4. The Γ–*R* relation

In the fitting procedure some parameters may degenerate given the interdependence among them. This is the case, for example of the photon index with the column density for low statistics observations. The same could happen for the determination of R and $E_{\rm c}$, since R introduces in the spectrum a bump peaking between 20–40 keV and declining at higher energies where the $E_{\rm c}$ may appear. To check if the results presented here are affected by such effects, the correlations between these parameters have been studied and the results are presented in Fig. 5.

The left panel of Fig. 5 shows how, on average, the estimate of Γ is not affected by the simultaneous determination of the absorbing column. No trend is observed between Γ and $N_{\rm H}$. Obviously, this does not imply that this is true for each single source included in the original sample. On the other hand, this is an expected result since the broad band of *BeppoSAX* should reduce this spurious effect. Similar results are obtained also when the Γ vs. $E_{\rm c}$, and R vs. $E_{\rm c}$ (center panel of Fig. 5) relations are investigated. In these cases the Spearman ρ and Kendall's τ tests do not support the existence of a relation between these quantities ($P_{\rm null} \sim 15\%$). All these indications suggest that, if any, the possible degeneracy in the fitting procedure did not introduce strong spurious relations between the spectral parameters.

However a strong correlation ($P_{\rm null} \leq 0.01\%$) is recorded between Γ and R (that are linked by the following relation):

$$R = (4.54 \pm 1.15) \times \Gamma - (7.41 \pm 4.51). \quad (2)$$

It is hard to determine if this correlation is the result of a systematic effect since it is possible that these two quantities degenerate in the fitting procedure. A flat power-law with small reflection could be described also by a steep power-law plus strong reflection. The absence of similar correlations between Γ and $E_{\rm c}$ and R vs. $E_{\rm c}$ seems to suggest that this correlation is real.

A similar relation was previously found using *Ginga* and *RXTE* data (Zdziarski et al. 1999; Gilfanov et al. 1999). Zdziarski et al. (1999) interpreted this as evidence of thermal Comptonization as the origin of X-rays providing that the optical-UV seed photons were mainly produced by the same material responsible for the reflected component. In this case the cooling rate of the hot corona is directly linked to the power-law slope. But the cooling rate is also related to the angle subtended by the reflector. This result is also in agreement with predictions of models that consider mildly relativistic outflows driven by magnetic flares (Beloborodov 1999). In general, Merloni et al. (2006) demonstrated that any geometry in which the hot, X-ray emitting plasma is photon starved (i.e. geometries of the accreting systems in which the accretion disk is only partially covered by the Comptonizing plasma such as patchy coronae, inner ADAF plus outer disks etc.) will produce hard X-ray spectra, little soft thermal emission and a weak reflection component. On the other hand, geometries corresponding to a very large covering fractions of the cold phase have strong soft emission, softer spectra and strong reflection fractions (Collin-Souffrin et al. 1996). Thus, moving along the Γ vs. R relation implies moving from lower to higher accreting systems.

5. Summary and conclusions

The average properties of Seyfert galaxies in the local Universe ($z \leq 0.1$) as seen by *BeppoSAX* was investigated, analyzing the

sample of objects presented in Dadina (2007). Multiple observations of single objects were treated independently, i.e. the multiple measurements of parameters were not averaged for statistical purposes. This method has been chosen since, in the framework of the simplest version of UM for AGN (Antonucci 1993) the AGN are thought to be very similar to each other and only orientation/absorption effects and the activity-level of the targets could introduce observational differences between different objects. In this scenario, the monitoring of a single source could be reproduced by the observations of many sources in different states and vice versa.

BeppoSAX offered the advantage of a useful X-ray broad energy band. Data studied here fall in the 2–100 keV band for the majority of objects. This advantage has been used to investigate the properties of the high-energy continuum of Seyfert galaxies. As stated in a previous paper (Dadina 2007), the basic template was a power-law with a high energy cut-off plus a reflection component (namely PEXRAV model in XSPEC). The results of this analysis can be summarized as follow:

- The average slope of the power-law is 1.84 ± 0.03 for the entire sample of objects. Considering the two families of AGN separately, $\Gamma = 1.89 \pm 0.03$ for type I objects (including Seyfert 1, 1.2 and 1.5) while $\Gamma = 1.80 \pm 0.05$ for type II objects (including Seyfert 1.8, 1.9 and 2).
- The average value of the relative reflected-to-direct normalization parameter R is 1.01 ± 0.09 with a slight difference between the two classes of Seyfert galaxies ($R = 1.23 \pm 0.11$ for type I objects and $R = 0.87 \pm 0.14$ for the type II ones).
- The high energy cut-off was measured to be $E_c = 287 \pm 24$ ($E_c = 230 \pm 22$ keV for Seyfert 1 and $E_c = 376 \pm 42$ keV for Seyferts 2).
- As expected and as known from previous works, the absorbing column is very different in the two classes of objects. On average $N_H \sim 3.66 \times 10^{22}$ cm^{-2} type I and $N_H \sim 6.13 \times 10^{23}$ cm^{-2} for type II AGN. The high mean value obtained for Seyfert 1 is caused by a selection effect induced by the energy coverage of the MECS+PDS instruments (2–100 keV).
- Evidence of a X-ray Baldwin effect is found in Seyfert 1 galaxies when the EW of the FeKα line is plotted against the 20–100 keV luminosity.
- A significant correlation has been found between R and Γ.

These results are well in agreement with the basic assumptions of the UM for AGN (Antonucci 1993). No differences are measured in the observables that are supposed to be isotropic while the absorbing column seems to be the only discriminator between the different types of Seyfert galaxies. This is reflected also in the properties of the FeKα line. No difference is measured in the line centroid (see Table 3) between the two classes of Seyfert galaxies. Type II objects, however, display more intense features ($EW = 222 \pm 33$ eV for Seyfert 1 and $EW = 693 \pm 195$ eV for Seyfert 2). The physical origin of the X-ray "Baldwin effect" here measured for Seyfert 1 using the 20–100 luminosity is unclear. Both light bending (Miniutti & Fabian 2004) and torus models (Page et al. 2004) are consistent with the present data even if the strong relation of the FeKα line EW in type II objects with the absorption column indicates that most of the narrow line component should be due to the torus. Finally, the measured Γ-R relationship is consistent with thermal Comptonization models.

Acknowledgements. I thank G. G. C. Palumbo and M. Cappi for helpful discussion and for careful reading of the previous versions of the manuscript. I also thank the ASDC staff for their wonderful work in mantaining the *BeppoSAX* database. I really thank the referee for her/his helpful comments and suggestions that contributed to improve the quality of the manuscript. Financial support from ASI is aknowledged.

References

Antonucci, R. 1993, ARA&A, 31, 473
Bassani, L., Dadina, M., Maiolino, R., et al. 1999, ApJS, 121, 473
Beloborodov, A. M. 1999, ApJ, 510, L123
Bianchi, S., Guainazzi, M., Matt, G., & Fonseca Bonilla, N. 2007, A&A, 467, L19
Boella, G., Chiappetti, L., Conti, G., et al. 1997, A&AS, 122, 327
Braito, V., Della Ceca, R., Piconcelli, E., et al. 2004, A&A, 420, 79
Cappi, M., Panessa, F., Bassani, L., et al. 2006, A&A, 446, 459
Collin-Souffrin, S., Czerny, B., Dumont, A.-M., & Zycki, P. T. 1996, A&A, 314, 393
Crenshaw, D. M., & Kraemer, S. B. 2007, ApJ, 659, 250
Czerny, B., Nikołajuk, M., Różańska, A., et al. 2003, A&A, 412, 317
Dadina, M. 2007, A&A, 461, 1209
De Rosa, A., Piro, L., Perola, G. C., et al. 2007, A&A, 463, 903
Farrah, D., Afonso, J., Efstathiou, A., et al. 2003, MNRAS, 343, 585
Feigelson, E. D., & Nelson, P. I. 1985, ApJ, 293, 192
Franceschini, A., Braito, V., Persic, M., et al. 2003, MNRAS, 343, 1181
Ghisellini, G., Haardt, F., & Matt, G. 1994, MNRAS, 267, 743
Gilfanov, M., Churazov, E., & Revnivtsev, M. 1999, A&A, 352, 182
Grandi, P., Malaguti, G., & Fiocchi, M. 2006, ApJ, 642, 113
Guainazzi, M., Nicastro, F., Fiore, F., et al. 1998, MNRAS, 301, L1
Haardt, F. 1993, ApJ, 413, 680
Haardt, F., & Maraschi, L. 1991, ApJ, 380, L51
Haardt, F., Maraschi, L., & Ghisellini, G. 1997, ApJ, 476, 620
Isobe, T., Feigelson, E. D., & Nelson, P. I. 1986, ApJ, 306, 490
Iwasawa, K., & Taniguchi, Y. 1993, ApJ, 413, L15
Jiang, P., Wang, J. X., & Wang, T. G. 2006, ApJ, 644, 725
Leahy, D. A., & Creighton, J. 1993, MNRAS, 263, 314
Lee, J. C., Fabian, A. C., Reynolds, C. S., Brandt, W. N., & Iwasawa, K. 2000, MNRAS, 318, 857
Magdziarz, P., & Zdziarski, A. A. 1995, MNRAS, 273, 837
Maiolino, R., Salvati, M., Bassani, L., et al. 1998, A&A, 338, 781
Makishima, K. 1986, The Physics of Accretion onto Compact Objects, LNP 266, 249
Malizia, A., Bassani, L., Stephen, J. B., et al. 2003, ApJ, 589, L17
Merloni, A., Malzac, J., Fabian, A. C., & Ross, R. R. 2006, MNRAS, 370, 1699
Miniutti, G., & Fabian, A. C. 2004, MNRAS, 349, 1435
Nandra, K. 2006, MNRAS, 368, L62
Page, K. L., O'Brien, P. T., Reeves, J. N., & Turner, M. J. L. 2004, MNRAS, 347, 316
Panessa, F., Bassani, L., Cappi, M., et al. 2006, A&A, 455, 173
Perola, G. C., Matt, G., Cappi, M., et al. 2002, A&A, 389, 802
Petrucci, P.-O., Dadina, M., & Landi, R., submitted to A&A
Ponti, G., Miniutti, G., Cappi, M., et al. 2006, MNRAS, 368, 903
Poutanen, J., & Svensson, R. 1996, ApJ, 470, 249
Ptak, A., Heckman, T., Levenson, N. A., Weaver, K., & Strickland, D. 2003, ApJ, 592, 782
Risaliti, G., Maiolino, R., & Salvati, M. 1999, ApJ, 522, 157
Risaliti, G., Elvis, M., & Nicastro, F. 2002, ApJ, 571, 234
Shih, D. C., Iwasawa, K., & Fabian, A. C. 2002, MNRAS, 333, 687
Smith, P. S., Schmidt, G. D., Allen, R. G., & Angel, J. R. P. 1995, ApJ, 444, 146
Turner, T. J., George, I. M., Nandra, K., & Turcan, D. 1999, ApJ, 524, 667
Véron-Cetty, M.-P., & Véron, P. 2006, A&A, 455, 773
Zdziarski, A. A., Lubinski, P., & Smith, D. A. 1999, MNRAS, 303, L11
Zhou, X.-L., & Wang, J.-M. 2005, ApJ, 618, L83